State tomography for magnetization dynamics

Tomosato Hioki, Hiroki Shimizu, Takahiko Makiuchi, and Eiji Saitoh

Phys. Rev. B **104**, L100419 — Published 30 September 2021

DOI: 10.1103/PhysRevB.104.L100419

Magnetization State Tomography

Tomosato Hioki,[1,2,*] Hiroki Shimizu,[2] Takahiko Makiuchi,[2] and Eiji Saitoh[1,2,3]

[1] *Advanced Institute for Materials Research, Tohoku University, Sendai 980-8577, Japan*
[2] *Department of Applied Physics, The University of Tokyo, Tokyo 113-8656, Japan*
[3] *Institute for AI and Beyond, The University of Tokyo, Tokyo 113-8656, Japan*

(Dated: September 14, 2021)

State tomography is an essential tool for analyzing physical states in quantum science. In magnets, elementary excitation called a magnon, or a spin wave, dominates magnetization dynamics and various magnetic properties. Here we propose and demonstrate state tomography for magnetization dynamics, enabling us to obtain a density matrix and Wigner function of magnetization dynamics. Using the technique, we found that parametrically excited magnons can form a mixed state composed of two coherent states. The magnetization state tomography will pave a way to explore a wide range of states of magnons, such as squeezed state in condensed matter.

In magnets, magnetization dynamical states can be described in terms of magnons. Magnons refer to elementary excitation of magnetization precessional motion, one of the major spin-current carriers in solids [1–3]. Recently, some exotic states of magnons characterized by unconventional fluctuation have theoretically been predicted, such as magnon squeezed states, mixed states, and entanglement between magnons [4–10]. In general, a state of a dynamical system can be characterized by an average and fluctuation of its representative variables. To investigate the dynamical states of magnetization or magnons, acquisition of density matrix for magnetization dynamics is thus expected. The density matrix has often been interpreted by using pseudo-probability distribution such as a Wigner function, which can visualize quantum and classical nature of the dynamics [11]. State tomography has been used as a fundamental method in quantum optics and quantum computation science to analyze the state of a photon or a superconducting qubit [12–14]. Realization of magnetization state tomography will thus open a way to investigate various magnon states in a wide range of magnetic materials.

Here we propose magnetization state tomography (MST), based on magnetization-fluctuation measurement at a fixed frequency. We also experimentally demonstrate magnetization state tomography for a Pt/YIG ($Y_3Fe_5O_{12}$) dot under parametric excitation, by showing the observation of a mixed state of magnons in the sample.

In the following, we formulate experimental observables for MST. To perform MST, it is necessary to measure marginal probability distribution $|\langle x_\theta|\psi_{f_0}\rangle|^2$ at a fixed frequency, f_0, which conveys the mean and fluctuation of magnon amplitude at f_0. Here, $|\psi_{f_0}\rangle$ is a magnon state (either mixed or pure state) at f_0 obtained by using a phase-sensitive measurement technique. $x_\theta = x\cos\theta + p\sin\theta$ is the amplitude around the measurement axis $\mathbf{x}_\theta$ in quadrature space defined by the quadrature operators $\hat{x} = \frac{1}{\sqrt{2}}\left(\hat{a} + \hat{a}^\dagger\right)$, $\hat{p} = \frac{1}{\sqrt{2}i}\left(\hat{a} - \hat{a}^\dagger\right)$. $\hat{a}$ and $\hat{a}^\dagger$ are the annihilation and creation operators of a magnon. The marginal probability distribution corresponds to the projection of a Wigner function onto a line along $\mathbf{x}_\theta$ in the quadrature space schematically shown in Fig. 1(a). For magnons, the quadrature amplitude corresponds to the $x-$ and $y-$components of magnetization, $\tilde{m}_x(\omega_0)$ and $\tilde{m}_y(\omega_0)$, on a rotating frame of reference with the precession frequency [Fig. 1(b)]. The phase-sensitive measurement for magnons can be performed by several methods in principle, such as microwave spectroscopy, spin pumping [15–19], magneto resistance (MR) [20–24], and magneto-optical measurements [25–27]. Spin pumping refers to the AC or DC

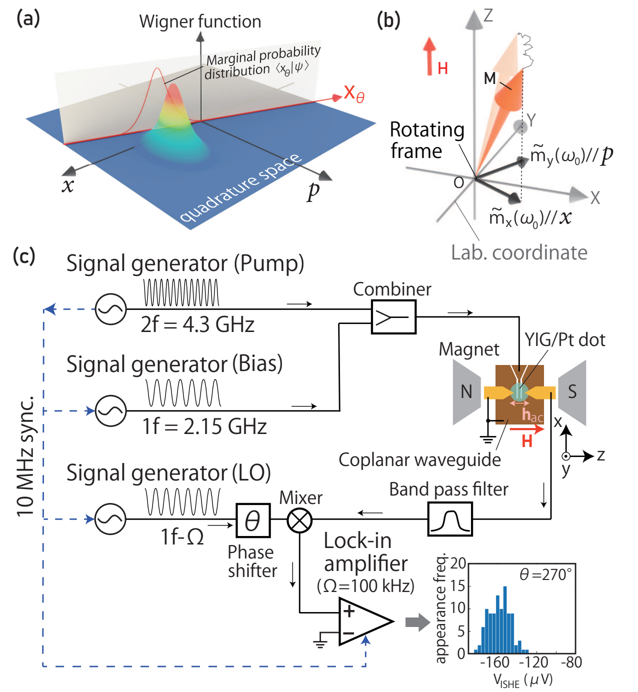

FIG. 1. (a) A schematic illustration of Wigner functions and marginal probability distribution in quadrature space. (b) Correspondence between quadrature amplitude and precession amplitude. (c) A schematic illustration of the measurement setup used in the present study.

* tomosato.hioki.d7@tohoku.ac.jp

spin-current generation at a normal-metal/ferromagnetic material interface as a result of magnetization precession. The generated spin current reflects the precession dynamics, realizing spin-pumping MST, while magneto-optical measurement can detect the magnetization precession component through a magneto-optical effect, such as the Faraday and Cotton–Mouton effects, and Brillouin light scattering [28, 29], realizing magneto-optical MST.

This paper describes spin-pumping MST in detail. In the case of AC spin-pumping measurement, the generated spin current density can be written as follows [17]

$$\mathbf{J}_{\mathrm{s}} = \frac{\hbar}{4\pi}\left[\mathrm{Re}g_{\uparrow\downarrow}\left(\mathbf{m}\times\dot{\mathbf{m}}\right) + \mathrm{Im}g_{\uparrow\downarrow}\dot{\mathbf{m}}\right], \qquad (1)$$

where $\mathbf{J}_{\mathrm{s}}$ is the generated spin current density, $\mathbf{m}$ is the magnetic moment normalized by the saturation magnetization M_{s}, $\hbar$ is the Dirac constant, and $\mathrm{Re}g_{\uparrow\downarrow}$ ($\mathrm{Im}g_{\uparrow\downarrow}$) is the real (imaginary) part of the spin mixing conductance. In the sample configuration shown in Fig. 1 (c), the y-component of the generated spin current density reads

$$J_{\mathrm{s}}^{y} = \frac{\hbar}{4\pi S_0^2}\left[\mathrm{Re}g_{\uparrow\downarrow}\left(\hat{S}_z\dot{\hat{S}}_x - \hat{S}_x\dot{\hat{S}}_z\right) + \mathrm{Im}g_{\uparrow\downarrow}\dot{\hat{S}}_y S_0\right], \quad (2)$$

where S_0 is the total spin density, $\hat{S}_i$ is the i-component of the spin operator. Here, we use the Holstein–Primakoff representation for a $k \simeq 0$ magnon at the linear order;

$$\hat{S}_+ = \hat{S}_x + i\hat{S}_y = \hbar\sqrt{\frac{2S_0}{V}}\hat{a}, \qquad (3)$$

$$\hat{S}_- = \hat{S}_x - i\hat{S}_y = \hbar\sqrt{\frac{2S_0}{V}}\hat{a}^{\dagger}, \qquad (4)$$

where V is the volume of the sample. By expanding the magnon operator to Fourier series, the spin current J_s^y is written as follows

$$J_{\mathrm{s}}^{y}(t) = i\tilde{s}_0\int_0^{\infty} d\omega\omega\left[\hat{a}(\omega)e^{i(\omega t+\phi)} - \hat{a}^{\dagger}(\omega)e^{-i(\omega t+\phi)}\right], \qquad (5)$$

where $\tilde{s_0}$ is defined as $\tilde{s_0} = \frac{\hbar}{4\pi\sqrt{2S_0V}}|g_{\uparrow\downarrow}|$, ϕ is a material-dependent phase factor for mixing conductance defined as follows $g_{\uparrow\downarrow} = |g_{\uparrow\downarrow}|e^{i\phi}$. The generated spin current is converted into an electric current via the inverse spin-Hall effect (ISHE) in the normal metal layer attached to the ferromagnet [15, 30–32]. The generated electric current via ISHE is written as follows

$$J_{\mathrm{c}}^{z}(t) = i\tilde{e}\int_0^{\infty} d\omega\omega\left[\hat{a}(\omega)e^{i(\omega t+\phi)} - \hat{a}^{\dagger}(\omega)e^{-i(\omega t+\phi)}\right]. \qquad (6)$$

$\tilde{e} = \frac{2e}{\hbar}\alpha_{\mathrm{N/F}}A\tilde{s_0}$ is the reduced electric charge. $\alpha_{\mathrm{N/F}}$ is the spin-Hall angle, and A is a factor to reduce a spin current reflecting the back flow of the spin current $A = \frac{\lambda_{\mathrm{N}}}{d_{\mathrm{N}}}\tanh\left(\frac{d_{\mathrm{N}}}{2\lambda_{\mathrm{N}}}\right)$, where λ_{N} and d_{N} are the spin diffusion length and the thickness of the normal-metal [18]. By analyzing the mean and fluctuation of J_{c}^{z}, we can estimate magnon marginal probability distribution by using Eq. (6).

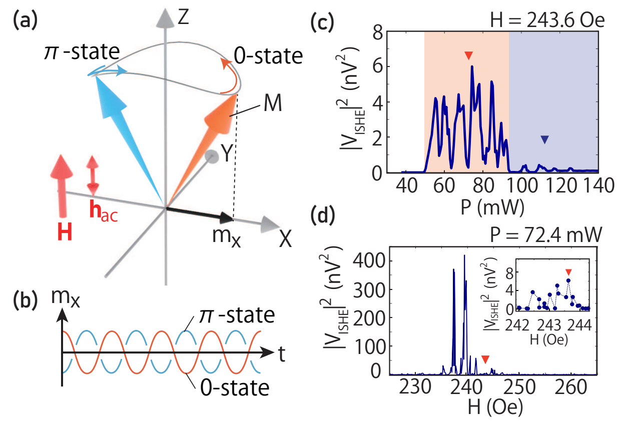

FIG. 2. (a) A schematic illustration of parametrically excited magnetization dynamics under the parallel parametric pumping. Magnetic moment precesses with the angular frequency of $\omega_0 = 2\pi f_0$ with the initial phase of 0 or π with respect to the pumping microwave. (b) A schematic illustration of the 0- and π-phase states plotted as a function of time t. m_x is the x-component of magnetization. (c) Power dependence of the AC inverse spin-Hall voltage. (d) Magnetic field dependence of the AC inverse spin-Hall voltage. The inset shows the voltage near $H = 243.6$ Oe, where we perform the MST measurement.

In the following, we demonstrate MST via the electric detection of magnetization dynamics based on the AC spin pumping and ISHE. We used a micro-meter-scale dot-shaped Pt/YIG bilayer sample, Pt is used for driving ISHE [33]. We employ homodyne technique to read the quadrature amplitude. The frequency of the generated AC ISHE voltage in the Pt layer is down-converted by using a mixer circuit driven by a synchronized signal generator, named a local oscillator (LO). The frequency of the LO is set to $f_0 - \Omega$ to realize homodyne detection of the signal with a lock-in amplifier of which the reference frequency is Ω. We use the operators $\hat{x}$ and $\hat{p}$ to map the magnon amplitude at the fixed frequency of $f_0 = \omega_0/2\pi$ to the quadrature amplitude, which leads to the following formula of the output signal,

$$V_{\mathrm{LI}}^{\mathrm{R}} = \sqrt{2}\rho w\tilde{e}|G_{\mathrm{p}}|\omega_0\left[\hat{p}\cos(\theta+\phi) - \hat{x}\sin(\theta+\phi)\right], \quad (7)$$

$$V_{\mathrm{LI}}^{\mathrm{I}} = \sqrt{2}\rho w\tilde{e}|G_{\mathrm{p}}|\omega_0\left[\hat{x}\cos(\theta+\phi) + \hat{p}\sin(\theta+\phi)\right], \quad (8)$$

where ρ is the resistivity of the Pt, w is the distance between the voltage electrodes on the Pt, G_{p} is the gain of the mixer, and θ is the relative phase between the output signal and the microwave from the LO. We measured the output signal with a lock-in amplifier with finite lock-in frequency, Ω =100 kHz, to eliminate 1/f noise. By measuring the $V_{\mathrm{LI}}^{\mathrm{R,I}}$ for statistical times, we obtain a appearance-frequency histogram for as a function of voltage value as shown in the inset to Fig. 1(c), which is regarded as marginal probability distribution of magnons. The measurement axis is rotated in the quadrature space by changing the phase θ to perform state tomography.

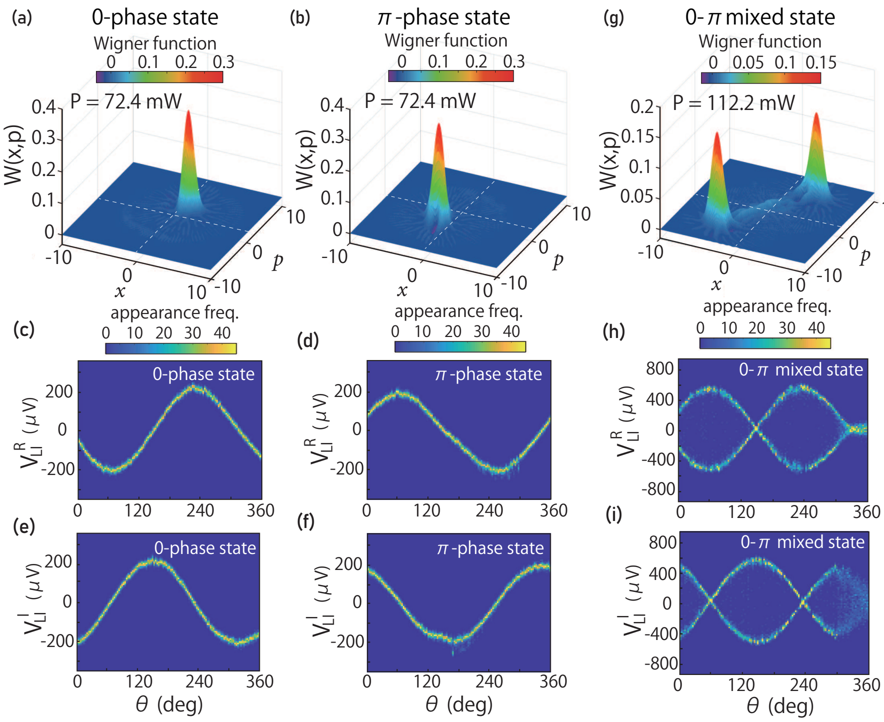

FIG. 3. (a) Reconstructed Wigner function for the experimentally obtained 0-phase state at the excitation power of 72.4 mW in the YIG/Pt dot. (b) Reconstructed Wiger function for the experimentally obtained π-phase state at 72.4 mW. (c)–(f) Contour plot of the appearance frequency distribution of the ISHE voltage. (c) and (d) show the distribution of the real part of the lock-in voltage ($V_{\mathrm{LI}}^{\mathrm{R}}$) for the 0- and π-phase states obtained at 72.4 mW. (e) and (f) show the imaginary part of the lock-in voltage ($V_{\mathrm{LI}}^{\mathrm{I}}$). (g) Reconstructed Wigner function for the experimentally obtained 0-π mixed state at 112.2 mW. (h) Contour plot of the appearance frequency distribution obtained by measuring $V_{\mathrm{LI}}^{\mathrm{R}}$ at 112.2 mW, (i) Contour plot of occurrence distribution obtained by measuring $V_{\mathrm{LI}}^{\mathrm{I}}$ at 112.2 mW. The noisy behavior of the data in the region where $\theta \geq 300^{\circ}$ is attributed to the temporary lack of the magnetic-field stability.

Theoretically, some unconventional magnon states have been predicted under parallel parametric excitation in a magnetic thin-film[8]. The parallel parametric excitation is driven by a microwave with the doubled frequency of the ferromagnetic resonance (FMR) frequency whose magnetic field component is parallel to the external field [34]. Owing to the shape magnetic anisotropy, the parametrically excited magnons can occupy either state: a 0-phase state or π-phase state, which can be distinguished by a relative phase with respect to the pumping microwave as schematically shown in Figs. 2(a) and (b). Since the two states are energetically degenerated, either 0- or π-phase state is probabilistically excited.

In the present study, we prepared the 130-μm-in-diameter dot sample by negative photo-lithography process from a Pt (10 nm)/YIG (370 nm) bilayer film. Both the Pt and YIG layers are prepared by sputtering in an ultrahigh vacuum [36]. The sample is mounted on coplanar waveguides to introduce a microwave and to detect the generated AC ISHE voltage [Fig. 2(c)]. The microwave magnetic field is parallel to the external magnetic field for parametric excitation of magnons. The pumping microwave frequency is set to $2f = 4.30$ GHz, and the microwave power is swept from 37.6 to 149.6 mW. Due to the parametric excitation, the precession oscillation frequency is the half of the pumping microwave frequency. We measured AC voltage generated in the Pt layer along the external field (z-axis) to detect the AC spin-pumping ISHE voltage. The voltage is measured 100 times per a single θ, and the increment of θ is three degrees. All the measurements were performed at room temperature.

We employed a maximum-likelihood method [37] to obtain the density matrix from the experimental data. The Wigner function was reconstructed from the density matrix [12] (See Supplemental Material). We renormalized magnon number by the factor of 10^{11}, as the typical magnon number under parametric excitation is as large as $\sim 10^{10}$ [38, 39]. We confirmed that the renormalization does not affect the obtained distribution of the number states.

We checked the condition of stable parametric excitation before the MST measurement. Figure 2(c) shows the power of the AC ISHE voltage as a function of the input $2f$ microwave (4.3 GHz) power, observed when the external magnetic field (243.6 Oe) almost satisfies the FMR condition for the frequency of $1f$ [Fig. 2(d)]. The ISHE voltage shows clear non-linear behavior with

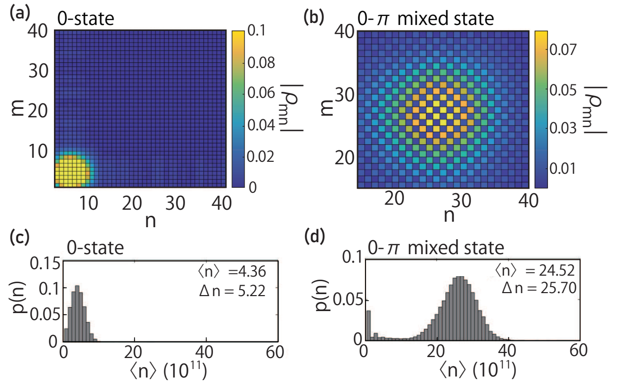

FIG. 4. (a) The absolute value of the density matrix for the experimentally obtained 0-state at 72.4 mW. (b) The absolute value of the density matrix for the experimentally obtained 0-π mixed state at 112.2 mW, which exhibits a characteristic chessboard pattern. (c) The number distribution for the 0-state. (d) The number distribution for the 0-π mixed state.

the threshold power of 49.0 mW. Above the microwave power of 94.0 mW, ISHE signal drops down due to the strong non-linearity in the magnetization dynamics [40]. The observed fine peak structures as a function of H can be attributed to the excitation of spin standing wave modes in the Pt/YIG dot [35, 41]. The peak magnetic field is 238.9 Oe, which coincides with the FMR field for $1f = 2.15$ GHz according to Kittel's equation (See Supplemental Material).

We performed the MST measurement at $H = 243.6$ Oe highlighted with an inverted triangle in Fig. 2(d), at which we found stable parametric oscillation. To excite either 0- or π-phase state selectively, we controlled the phase of a weak bias microwave with the frequency of $1f = 2.15$ GHz, which is applied when the $2f$ microwave is switched on. In Fig. 3(a), we show Wigner function reconstructed from the data obtained under the pumping microwave power of 72.4 mW. The result exhibits a single peak in the right-top (first) quadrant, signaling a 0-phase state. On the other hand, Wigner function reconstructed from another data exhibits a peak in the left-bottom (third) quadrant as shown in Fig. 3(b), signaling a π-phase state. The relative phase difference between the two states is π, consistent with the property of parametrically excited magnons.

Figure 3(c) shows the frequency distribution of $V_{\rm LI}^{\rm R}$ as a function of θ under the excitation of 0-phase. The peak of the frequency distribution follows sinusoidal dependence, consistent with Eq. (7). Under the excitation of π-phase, on the other hand, the distribution of $V_{\rm LI}^{\rm R}$ follows sinusoidal dependence with the opposite sign with respect to that of the 0-phase excitation [Fig. 3(d)]. Figures 3(e) and (f) show the frequency distributions of $V_{\rm LI}^{\rm I}$ under the excitation of the 0- and π-phase states, respectively. The $V_{\rm LI}^{\rm I}$ follows cosine-like θ dependence, consistent with Eq. (8).

We estimated magnon number from the voltage amplitude [44]. The ISHE parameters and $g_{\uparrow\downarrow} = 1.94 \times 10^{18}$ m^{-2} are estimated from DC spin-Hall measurement for the same sample (See Supplemental Material). The voltage peak for the 0-phase state is 210 μV, signaling the magnon number of 4.2×10^{11}, which is reasonably matches with the previous theoretical researches [42, 43]. The number corresponds to the precession angle of $\sim$4.7 degrees.

Figure 3(g) shows the experimentally obtained Wigner function for magnons parametrically excited by a 112.2-milliwatt microwave without bias microwaves. In the condition, due to the strong non-linearity, the steady 0- or π-phase signals disappear and the ISHE voltage fluctuates. We found that the obtained Wiger function for the 112.2-milliwatt excitation shows two peaks with similar amplitude, a characteristic feature for a mixed state. The relative phase between the two peaks is π, which demonstrates the formation of a mixed state made up of 0- and π-phase states under such strong parametric excitation. Figures 3 (h) and (i) show the obtained appearance frequency distribution under the condition, which can be interpreted as a sum of two frequency distributions of 0- and π-phase states.

Figure 4(a) shows the experimentally obtained density matrix for the 0-phase state. The density matrix for the 0-phase state shows Gaussian distribution [Fig. 4(c)] on the number basis, experimentally demonstrating the formation of single coherent state as a result of parametric excitation. On the other hand, as shown in Fig. 4(b), the experimentally obtained density matrix for the 0-π mixed state at 112.2 mW was found to exhibit a characteristic chessboard pattern on the number basis. Theoretically, a density matrix element for a 0-π mixed state is given by

$$\rho_{mn} = e^{-|\alpha|^2} \frac{\alpha^n \alpha^{*m}}{\sqrt{n!}\sqrt{m!}} \left[1 + (-1)^{m+n}\right], \tag{9}$$

where m and n are the magnon number indices, and α is complex amplitude of a magnon coherent state [46]. When $m+n$ is an odd (even) number, $\rho_{mn} = 0$ ($\rho_{mn} \neq 0$). Equation (9) well reproduces the experimentally obtained chessboard pattern shown in Fig. 4(b). The result provides evidence that our state tomography properly measures the density matrices for the magnetization dynamics. Note that the peak at $\langle n\rangle = 0$ of number distribution in Fig. 4(d) is an experimental artifact due to the unstable voltage seen in the region $300° < \theta < 360°$ in Figs. 3(h) and (i), which we attribute to a temporary lack of magnetic field stability.

In summary, we proposed and experimentally demonstrated the magnetization state tomography by measuring AC voltage generated by parametrically excited magnons via the AC spin pumping and the inverse spin-Hall effect. The obtained Wigner functions and density matrices on the number basis demonstrate that the parametric excitation of magnon can leads to the formation of a mixed state made up of two coherent states with the opposite phases. The magnetization state tomography gives an access to density matrices of various magnon states in a wide range of magnetic materials.

ACKNOWLEDGMENTS

We thank N. Yokoi, B. Hillebrands, and V. I. Vasyuchka for fruitful discussions. This work was financially supported by JST-ERATO Grant Number JPMJER1402, JST ERATO Grant Number JPMJER1402, Japan, and JSPS KAKENHI (Grant Numbers JP19H05600 and JP20K15160), Japan, and JST CREST (Nos. JPMJCR20C1, JPMJCR20T2), Japan.

---

[1] Y. Kajiwara, K. Harii, S. Takahashi, J. Ohe, K. Uchida, M. Mizuguchi, H. Umezawa, H. Kawai, K. Ando, K. Takanashi, S. Maekawa and E. Saitoh, Nature, **464**, 262-266 (2010).

[2] G. E. W. Bauer, E. Saitoh, and B. J. van Wees, Nat. Mater. **11**, 391-399 (2012).

[3] A. V. Chumak, V. I. Vasyuchka, A. A. Serga and B. Hillebrands, Nat. Phys. **11**, 453-461 (2015).

[4] M. Elyasi, Y. M. Blanter, and G. E. W. Bauer, Phys. Rev. B **101**, 054402 (2020).

[5] J. Zou, S. K. Kim, and Y. Tserkovnyak, Phys. Rev. B **101**, 014416 (2020).

[6] J. Li, S. Y. Zhu, and G. S. Agarwal, Phys. Rev. A **99**, 021801(R) (2019).

[7] M. Kostylev, A. B. Ustinov, A. V. Drozdovskii, B. A. Kalinikos, and E. Ivanov, Phys. Rev. B **100**, 020401(R) (2019).

[8] Z. Haghshenasfard and M. G. Cottam, J. Phys.: Condens. Matter **29**, 045803 (2016).

[9] Z. Zhang, M. O. Scully, and G. S. Agarwal, Phys. Rev. Research, **1**, 023021 (2019).

[10] A. Kamra, E. Thingstad, G. Rastelli, R. A. Duine, A. Brataas, W. Belzig, and A. Sudbø Phys. Rev. B **100**, 174407 (2019).

[11] M. Hillery, R. F. O'Connell, M. O. Scully, and E. P. Wigner, Phys. Rep. 106, 122-167 (1984).

[12] Ulf Leonhardt, *"Measuring the Quantum State of Light"*, (Cambridge University Press, 1997).

[13] G. M. D'Ariano, C. Macchiavello, and M. G. A. Paris, Phys. Rev. A **50**, 4298 (1994).

[14] K. Vogel and H. Risken, Phys. Rev. A **40**, 2847 (1989).

[15] E. Saitoh, M. Ueda, and H. Miyajima, Appl. Phys. Lett. **88**, 182509 (2006).

[16] D. Wei, et al., Nat. Commun. **5**, 3768 (2014).

[17] H. J. Jiao, and G. E. W. Bauer, Phys. Rev. Lett. **110**, 217602 (2013).

[18] K. Ando, S. Takahashi, J. Ieda, Y. Kajiwara, H. Naklayama, T. Yoshino, K. Harii, Y. Fujikawa, M. Matsuo, S. Maekawa, and E. Saitoh, J. Appl. Phys. **109**, 103913 (2011).

[19] H. Nakayama, K. Ando, K. Harii, T. Yoshino, R. Takahashi, Y. Kajiwara, K. Uchida, and Y. Fujikawa, and E. Saitoh, Phys. Rev. B **85**, 144408 (2012).

[20] E. H. Hall, Phil. Mag. **10**, 301 (1880).

[21] N. Nagaosa, J. Sinova, S. Onoda, A. H. MacDonald, and N. P. Ong, Rev. Mod. Phys. **82**, 1539 (2010).

[22] H. J. Juretschke, J. Appl. Phys **31**, 1401 (1960).

[23] G. Binasch, P. Grünberg, F. Saurenbach, and W. Zinn, Phys. Rev. B **39**, 4828 (1989).

[24] M. N. Baibich, J. M. Broto, A. Fert, F. Nguyen Van Dau, F. Petroff, P. Etienne, G. Creuzet, A. Friederich, and J. Chazelas, Phys. Rev. Lett. **61**, 2472 (1988).

[25] Y. Hashimoto, S. Daimon, R. Iguchi, Y. Oikawa, K. Shen, K. Sato, D. Bossini, Y. Tabuchi, T. Satoh, B. Hillebrands, G. E. W. Bauer, T. H. Johansen, A. Kirilyuk, T. Rasing, and E. Saitoh, Nat. Commun. **8**, 15859 (2017).

[26] T. Satoh, Y. Terui, R. Moriya, B. A. Ivanov, K. Ando, E. Saitoh, T. Shimura, and K. Kuroda, Nat. Photon. **6**, 662-666 (2012).

[27] T. Hioki, Y. Hashimoto, and E. Saitoh, Commun. Phys. **3**, 188 (2020).

[28] O. Büttner, M. Bauer, S. O. Demokritov, B. Hillebrands, Y. S. Kivshar, V. Grimalsky, Y. Rapoport, and A. N. Slavin, Phys. Rev. B **61**, 11576 (2000).

[29] F. Fohr, A. A. Serga, T. Schneider, J. Hamrle, and B. Hillebrands, Rev. Sci. Instr. **80**, 043903 (2009).

[30] M. V. Costache, M. Sladkov, S. M. Watts, C. H. van der Wal, and B. J. van Wees, Phys. Rev. Lett. **97**, 216603 (2006).

[31] S. O. Valenzuela and M. Tinkham, Nature **442**, 176 (2006).

[32] T. Kimura, Y. Otani, T. Sato, S. Takahashi, and S. Maekawa, Phys. Rev. Lett. **98**, 156601 (2007).

[33] S. Takahashi, E. Saitoh, and S. Maekawa, J. Phys.: Conf. Ser. **200**, 062030 (2010).

[34] T. Brächer, P. Pirro, and B. Hillebrands, Phys. Rep. **699**, 1 (2017).

[35] T. Makiuchi, T. Hioki, Y. Shimazu, Y. Oikawa, N. Yokoi, S. Daimon, and E. Saitoh, Appl. Phys. Lett. **118** 022402 (2021).

[36] T. Nozue T. Kikkawa, T. Watamura, T. Niizeki, R. Ramos, E. Saitoh, and H. Murakami, Appl. Phys. Lett. **113**, 262402 (2018).

[37] A. I. Lvovsky, J. Opt. B: Quantum Semiclass. Opt. **6**, S556 (2004).

[38] H. G. Bauer, P. Majchrak, T. Kachel, C. H. Back, and G. Woltersdorf, Nat. Commun. **6**, 8274 (2015).

[39] B. A. Auld, J. Appl. Phys **36**, 689 (1965).

[40] S. M. Rezende and F. M. de Aguiar, Proc. IEEE **78**, 893-908, (1990).

[41] F. Guo, L. M. Belova, and R. D. McMichael, Phys. Rev. B **89**, 104422 (2014).

[42] C. B. de Araujo, Phys. Rev. B **10**, 3961 (1974).

[43] *Fundamentals of Magnonics*, edited by L. Scalone (Springer Nature Switzerland AG, 2020).

[44] Z. Qiu, K. Ando, K. Uchida, Y. Kajiwara, R. Takahashi, H. Nakayama, T. An, Y. Fujikawa, and E. Saitoh, Appl. Phys. Lett. **103**, 092404 (2013).

[45] R. J. Glauber, Phys. Rev. **131**, 2766 (1963).

[46] S. M. Rezende, N. Zagury, Phys. Lett. A **29**, 1, 47-48 (1969).

[47] See Supplemental Material at [URL will be inserted by

publisher] for detail of estimation of spin mixing conductance, voltage-precession angle correspondence and method for reconstructing Wigner function from a density matrix. All files related to a published paper are stored as a single deposit and assigned a Supplemental Material URL. This URL appears in the article's reference list.